Lipolysis in Brown Adipocytes Is Not Essential for Cold-Induced Thermogenesis in Mice

Hyunsu Shin[1,2], **Yinyan Ma**[1,3], **Tanya Chanturiya**[3], **Qiang Cao**[4], **Youlin Wang**[1,2], **Anil K.G. Kadegowda**[1], **Rachel Jackson**[1], **Dominic Rumore**[1], **Bingzhong Xue**[4], **Hang Shi**[4], **Oksana Gavrilova**[3], and **Liqing Yu**[1,2,5,*]

[1]Department of Animal and Avian Sciences, University of Maryland, College Park, MD 20742

[2]Center for Molecular and Translational Medicine, Institute for Biomedical Sciences, Georgia State University, Georgia, Atlanta, GA 30303

[3]The National Institute of Diabetes and Digestive and Kidney Diseases, National Institutes of Health, Bethesda, MD 20892

[4]Department of Biology, Center for Obesity Reversal, Georgia State University, Atlanta, GA 30303

Summary

Lipid droplet (LD) lipolysis in brown adipose tissue (BAT) is generally considered to be required for cold-induced nonshivering thermogenesis. Here we show that mice lacking BAT Comparative Gene Identification-58 (CGI-58), a lipolytic activator essential for the stimulated LD lipolysis, have normal thermogenic capacity and are not cold sensitive. Relative to littermate controls, these animals had higher body temperatures when they were provided food during cold exposure. The increase in body temperature in the fed, cold-exposed knockout mice was associated with increased energy expenditure and increased sympathetic innervation and browning of white adipose tissue (WAT). Mice lacking CGI-58 in both BAT and WAT were cold sensitive, but only in the fasted state. Thus, LD lipolysis in BAT is not essential for cold-induced nonshivering thermogenesis *in vivo*. Rather CGI-58-dependent LD lipolysis in BAT regulates WAT thermogenesis, and our data uncover an essential role of WAT lipolysis in fueling thermogenesis during fasting.

Graphical abstract

Lipolysis in brown fat is generally considered to be required for cold-induced thermogenesis. Shin et al. show that mice defective in brown fat lipolysis are not cold sensitive. These animals
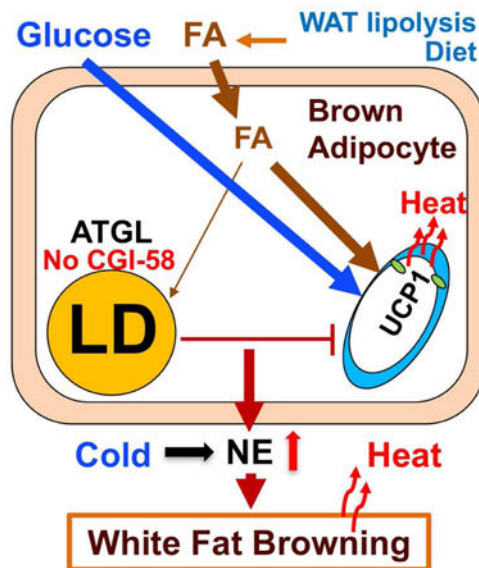
---

*To whom correspondence should be addressed: Liqing Yu, M.D., Ph.D., Lyu68@gsu.edu.
[5]Lead Contact

compensate for the defect by increasing white fat browning and combustion of fuels derived from diet or white fat lipolysis.

Introduction

Adipose tissue can be broadly divided into two types, brown adipose tissue (BAT) and white adipose tissue (WAT). Besides their endocrine functions, BAT and WAT mainly function to dissipate and store energy, respectively, in response to environmental and nutritional fluctuations. While rodents and human infants have visible classical BAT depots, it was once thought that adult humans lack BAT. Recent re-discovery of BAT-like tissue in adult humans by positron emission tomography (PET)-scanning has revitalized interest in basic and clinical research of BAT biology (Cypess et al., 2009; van Marken Lichtenbelt et al., 2009; Virtanen et al., 2009). A major function of BAT is to defend against cold in a nonshivering manner by generating heat from free fatty acids (FFAs), glucose and perhaps other chemicals (Cannon and Nedergaard, 2004; Kazak et al., 2015; Ozaki et al., 2011; Shabalina et al., 2013). Uncoupling protein 1 (UCP1) plays a key role in this adaptive thermogenesis by uncoupling mitochondrial oxidation of substrates from ATP synthesis (Cannon and Nedergaard, 2004).

Recently a distinct population of adipocytes that exist in WAT, contain multilocular lipid droplets (LDs), and express UCP1 were named brown-like (beige) or brown-in-white (brite) adipocytes (Petrovic et al., 2010; Wu et al., 2012). Although their origins are under debate, these cells are functionally thermogenic (Shabalina et al., 2013). The process of beige adipocyte recruitment to WAT is called WAT browning, which is often induced by cold exposure or stimulation with a sympathetic agonist (Nedergaard and Cannon, 2014; Rosen and Spiegelman, 2014). Rodents clearly have "classical" brown and beige/brite adipocytes. Humans may also possess both (Jespersen et al., 2013), or largely beige adipocytes (Sidossis and Kajimura, 2015).

BAT activity is mainly controlled by Sympathetic Nervous System (SNS) (Cannon and Nedergaard, 2004). Stimulation of SNS releases norepinephrine (NE), which raises intracellular cyclic AMP (cAMP) levels by activating adenylyl cyclase in the adrenergic signaling pathway. In mature brown adipocytes, NE-induced formation of cAMP seems to be fully mediated via β3-adrenergic receptor (Zhao et al., 1994). Thus, a selective β3 agonist CL316,243 is often used to mimic cold exposure to activate BAT activity. Increases in cellular cAMP activate protein kinase A (PKA) that phosphorylates a transcriptional factor cAMP-response-element binding protein (CREB) (Thonberg et al., 2002), resulting in transcriptional activation of thermogenic genes including UCP1 (Kozak et al., 1994). Activation of PKA stimulates cytosolic LD lipolysis (Honnor et al., 1985) that supposedly provides FFAs for brown adipocytes to produce heat. Thus, cytosolic LD lipolysis in brown adipocytes is generally considered to be required for cold-induced nonshivering thermogenesis (Cannon and Nedergaard, 2004). However, this concept has not been directly tested *in vivo* due to lack of appropriate animal models.

To address this long-outstanding issue, we created BAT-specific Comparative Gene Identification-58 (CGI-58) knockout (BAT-KO) mice. CGI-58, also known as Abhd5 (the fifth member of α/β-hydrolase fold protein family), is a LD-associated protein that is critically implicated in cytosolic LD lipolysis through interacting with LD coat proteins (Liu et al., 2004; Subramanian et al., 2004; Yamaguchi et al., 2004) and serving as a coactivator of Adipose Triglyceride Lipase (ATGL) (Lass et al., 2006). Like ATGL, CGI-58 is ubiquitously expressed with the highest expression in adipose tissue (Lass et al., 2006; Subramanian et al., 2004). In this study, we found that BAT-KO mice were not cold sensitive even in the fasted state. They expressed relatively normal levels of UCP1 mRNA and protein in the interscapular BAT (iBAT) under the basal condition, and had normal thermogenic capacity. Interestingly, BAT-KO mice showed increased combustion of circulating fuel and augmented browning of the inguinal subcutaneous fat (iWAT). In addition, we found that mice lacking CGI-58 in both BAT and WAT (FAT-KO mice) were cold sensitive in the fasted, but not fed state, which was different from previous studies that concluded that LD lipolysis is essential for cold-induced thermogenesis and brown phenotype (Ahmadian et al., 2011; Haemmerle et al., 2006). Comparison of cold tolerance between BAT-KO and FAT-KO mice revealed an essential role of WAT lipolysis in cold adaptation during fasting. Thus, our studies establish a new paradigm that LD lipolysis in brown adipocytes is not essential for sustaining brown phenotype and cold-induced non-shivering thermogenesis, but critically regulates BAT fuel sources and WAT thermogenesis during cold adaptation.

Results

Selective Inactivation of CGI-58 in BAT Induces iBAT Steatotic Hypertrophy and Hyperplasia

To identify the role of brown adipocyte LD lipolysis in thermoregulation and metabolic health, we generated BAT-KO mice by crossing CGI-58-floxed mice (Guo et al., 2013) with UCP1-cre transgenic mice (Kong et al., 2014). As reported by others using the same Cre mouse line, BAT-specific deletion was achieved (Figure S1A). At room temperature (22°C), BAT-KO versus control mice on chow or HFD gained weight similarly (Figure 1A) and had

similar energy intake (Figure 1B). They appeared grossly normal except a visible hump on the upper back, which was caused by enlarged iBAT that appeared like WAT (Figure 1C). The white fat appearance was attributable to large cytosolic LD accumulation resulting in a ~2-fold increase of average adipocyte size (steatotic hypertrophy) (Figure 1D and 1E). In addition, the total amount of DNA per iBAT increased ~2-fold in BAT-KO mice relative to littermate controls (Figure 1F), and a similar change was observed in iBAT protein (Figure 1G), suggesting an increase of the total cell number (hyperplasia) in CGI-58-deficient iBAT. Steatotic hypertrophy and hyperplasia together resulted in a ~4-fold increase of its weight on average (Figure 1H). Increased BAT weight did not increase fat body composition in BAT-KO mice (Figure S1B), which likely attributed to significant decreases in weights of white fat depots, including iWAT, epididymal WAT (eWAT) and mesenteric WAT (mWAT), though not peri-renal WAT (pWAT) (Figure 1H). As expected, the TG content increased ~2-fold in CGI-58-deficient iBAT (Figure 1I). Interestingly, the TG content decreased in iWAT and mWAT (Figure 1I) implying a compositional change of these fat depots in BAT-KO mice. Decreased WAT mass and TG content may contribute to reduced capacity of these animals to release FFAs and glycerol following lipolytic stimulation by isoproterenol (Figure 1K), but fold increases in FFA and glycerol release after isoproterenol injection were similar between the two genotypes (Figure 1K), suggesting that WAT's responsiveness to lipolytic stimulation is reserved in BAT-KO mice.

The Stimulated Lipolysis Is Abolished in CGI-58-Deficient iBAT

As mentioned under the Introduction, CGI-58 involves at least two steps of cytosolic LD lipolysis: i) interacting with LD coat proteins (perilipins), and ii) activating ATGL as a coactivator. Consequently, CGI-58 and ATGL mutations cause overlapping, yet distinct phenotypes (Fischer et al., 2007; Lord et al., 2016). In test tubes, CGI-58-deficient iBAT homogenates had significantly reduced lipase activity, which was further suppressed, though not significantly, by an ATGL inhibitor Atglistatin (Figure S1C). This finding was not surprising given the presence of ATGL protein in the homogenate of CGI-58-deficient iBAT (Figure S1D) and relatively low levels of CGI-58 expression in other cell types that constitutes ~50% of BAT (Rosenwald et al., 2013). Consistent with a previous study showing a major contribution of hormone sensitive lipase (HSL) to the *in vitro* lipase activity of adipose tissue homogenates (Schweiger et al., 2006), the predominant lipase activity in the homogenates of CGI-58-deficient and control iBATs was from HSL (Figure S1E), which is capable of hydrolyzing TG *in vitro* (Sztalryd et al., 1995). Despite abundant HSL and ATGL proteins in the homogenate of CGI-58-deficient iBAT (Figure S1D), CGI-58 deficiency, like ATGL or HSL inhibitor treatment, completely abolished forskolin-stimulated lipolysis in live iBAT explants (Figure 1J and S1F) demonstrating an essential role of CGI-58, ATGL, or HSL in mediating the stimulated lipolysis.

BAT-KO Mice Have Normal Energy Expenditure and Body Temperature at Room Temperature or Thermoneutrality

A major function of BAT is to dissipate energy as heat. However, BAT-KO mice only showed a minor reduction in total energy expenditure at room temperature (22°C) (Figure S1G). There were no significant differences in oxygen consumption, respiratory exchange ratio (RER, indicative of metabolic substrate preference), total physical activity, food intake,

and core body temperature between BAT-KO and control mice housed at either room temperature or thermoneutrality (30°C) (Figure S1G). As expected, thermoneutrality reduced total energy expenditure and oxygen consumption and increased RER in normal mice. Similar responses were observed in BAT-KO mice (Figure S1G). These findings demonstrate that LD lipolysis in BAT has limited impact on whole-body energy balance and thermogenesis at room temperature or thermoneutrality.

BAT-KO Mice Are Not Cold Sensitive

At room temperature, BAT-KO mice did not develop hypothermia even during fasting (Figure 2A). To determine whether defective LD lipolysis in BAT influences cold-induced thermogenesis under different nutritional status, we subjected chow-fed BAT-KO mice to acute cold exposure (4°C) and monitored changes in intra-rectal temperatures. BAT-KO mice were not cold sensitive when food was absent (Figure 2B). Relative to littermate controls, these animals had higher body temperatures when they were provided food during acute cold exposure (Figure 2C). Similar responses were observed in HFD-fed mice when the core body temperature was continuously monitored by Telemetry (Figure 2D and 2E). During chronic cold exposure when mice had free access to food and water, the core body temperature was significantly higher in the first 2 days, and stayed at a slightly higher level thereafter in BAT-KO mice than controls (Figure 2F). In addition, relative to littermate controls, BAT-KO mice had higher total energy expenditure during chronic, though not acute, cold exposure (Figure S2A), which was not a result of increased physical activity (Figure S2B).

CGI-58 Deletion in BAT Does Not Reduce Whole-Body Thermogenic Capacity

It was reported that iBAT UCP1 expression was reduced in mice lacking ATGL in all adipose tissues (Ahmadian et al., 2011). However, we did not observe a significant reduction of UCP1 protein in the iBAT of BAT-KO mice on chow (Figure 3A). Due to a ~50% increase of the total protein per iBAT in BAT-KO mice relative to the controls (Figure 1G), the total amount of UCP1 protein per iBAT was actually increased in these mice. To gain additional information as to why mice deficient in BAT lipolysis are not cold sensitive, we measured iBAT expression levels of UCP1 and other genes relevant to thermogenesis in mice treated with the β3 agonist CL316,243 for 4 days or cold for 7 days. Under the basal condition, *i.e.*, at room temperature without β3 agonist or cold treatment, iBAT UPC1 mRNA and protein levels did not differ between the two genotypes (Figure 3B-3E). The protein expression of tyrosine hydroxylase (TH), a marker of sympathetic innervation (Foster and Bartness, 2006), increased substantially in the CGI-58-deficient iBAT (Figure 3D) suggesting augmented sympathetic drive, which may partly explain its hyperplasic phenotype (Figure 1F) and reserved UCP1 expression. CGI-58 ablation in BAT also had no effects on iBAT levels of mRNAs for peroxisome proliferator-activated receptor (PPAR)-α, PR domain-containing 16 (PRDM16), and PPAR-γ, but increased iBAT levels of mRNAs for PPAR-γ coactivator (PGC)-1α and type II iodothyronine deiodinase (Dio2) (Figure 3B). Despite this, UCP1 protein expression in the CGI-58-deficient iBAT did show a blunted response to β3 agonist (Figure 3C) or cold (Figure 3D), which was not correlated with levels of mRNA for β3 adrenergic receptor (Figure S3A). Multiple transcriptional factors are implicated in transcriptional regulation of UCP1, including fatty acid-activated PPARα and

PGC-1α. The response of PPARα and PGC-1α to β3 agonist was also attenuated (Figure 3B). CGI-58 deficiency may suppress PPAR signaling in BAT by limiting PPAR ligands from cytosolic LD lipolysis as seen in the ATGL-deficient heart (Haemmerle et al., 2011). Nonetheless, attenuated UCP1 expression under cold did not reduce total energy expenditure (Figure S2A).

Cold-acclimated UCP1-deficient mice were able to defend body temperature via shivering-induced thermogenesis (Golozoubova et al., 2001). To eliminate muscle shivering and assess nonshivering thermogenic capacity in BAT-KO mice, we injected a bolus of the β3 agonist CL316,243 into the mice housed at thermoneutrality. BAT-KO and control mice had similar increases in core body temperatures (Figure 3F) within 3 h of injection. Although the average increase in oxygen consumption per mouse was significantly lower (~20% less) in BAT-KO mice than controls (Figure 3G) during this period, it reached the 2-fold level normally seen in CL316,243-injected mice (Grujic et al., 1997). When fold changes in oxygen consumption rates were plotted as a function of body weight or fat body mass that showed a trend towards decrease in BAT-KO mice, the difference was not statistically significant (Figure S3B). The modest reduction of CL316,243-stimulated oxygen consumption and FFA release (Figure 3H) in BAT-KO mice likely resulted from their reduced reserve of white fat (Figure 1H), a fat type whose β3 adrenergic receptor was reported to play a predominant role in determining total energy expenditure levels in mice following β3 agonist stimulation (Grujic et al., 1997). Importantly, isolated CGI-58-deficient primary brown adipocytes had no changes in basal and maximum oxygen consumption and responded to isoproterenol similarly as controls under normal Seahorse assay conditions (Figure 3I). When FFAs were completely depleted in the assay medium by adding a very high concentration (2%) of fatty acid-free albumin, the isoproterenol-stimulated and maximum oxygen consumption started to show a significant suppression in CGI-58-deficient brown adipocytes (Figure S3C). This observation is consistent with a previous study using ATGL and HSL inhibitors (Li et al., 2014) and suggests that CGI-58-mediated cytosolic LD lipolysis becomes critical in fueling brown adipocyte mitochondrial respiration only when exogenous FFAs are not available, a condition that does not normally occur *in vivo*. Overall, our results demonstrate that inhibiting the stimulated LD lipolysis in BAT does not reduce thermogenic capacity *in vivo* in mice.

BAT-KO Mice Increase Combustion of Circulating Fuels During Cold Exposure

Brown adipocytes may directly use FFAs, glucose and other chemicals derived from the blood as thermogenic substrates without firstly storing them in cytosolic LDs, though it was reported that utilization of TGs stored in cytosolic LDs of brown adipocytes plays a predominant role in acute cold-induced thermogenesis (Ma and Foster, 1986; Ouellet et al., 2012). In the fed state, diet is a major source of energetic substrates present in the blood. BAT-KO mice had increased calorie intake during chronic cold exposure (Figure 4A). The respiratory exchange ratio (RER) was significantly higher in these animals during the first 5 days of cold exposure (Figure 4B) indicating increased combustion of carbohydrates during this period. To provide direct evidence for this, we examined glucose-initiated thermogenesis during acute cold exposure. After a bolus of glucose, BAT-KO mice relative to controls showed a markedly attenuated response in blood glucose increases and a

significant rise in intra-rectal temperatures (Figure 4C and 4D). These results were consistent with increased glucose uptake by iWAT and by iBAT as an organ during cold exposure (Figure 4E). It was also consistent with increased mRNA for glucose transporter 1 (Glut1) in these fat depots (Figure 4F and S4A). The mRNA level of glucose transporter 4 (Glut4), which is responsible for insulin-stimulated glucose uptake, decreased in iBAT and remained unchanged in iWAT in BAT-KO mice (Figure 4F and S4A). Insulin-stimulated glucose uptake per mg wet tissue was not significantly altered in adipose and muscle tissues (Figure S4B), except CGI-58-deficient iBAT whose total glucose uptake should be considered elevated because of its increased wet weight.

Compared to glucose, FFAs are energy-rich molecules and normally the major fuel for thermogenesis. CD36, lipoprotein lipase (LPL) and fatty acid transporter 1 (FATP1) play important roles in iBAT uptake and transport of FFAs (Bartelt et al., 2011; Wu et al., 2006). We observed that iBAT levels of mRNAs for CD36 and LPL, but not FATP1, increased significantly in BAT-KO mice (Figure 4G). Expression of CD36 protein, a fatty acid transporter critically implicated in cold-induced thermogenesis (Bartelt et al., 2011), also elevated in the iBAT of BAT-KO mice after chronic cold exposure or CL316,243 treatment (Figure 4H). These findings imply that CGI-58-deficient BAT may have increased fatty acid uptake from the blood, especially during chronic cold adaptation. Collectively our results suggest that CGI-58-deficient BAT may compensate its defective LD lipolysis by increasing combustion of blood fuels including glucose and perhaps FFAs for thermogenesis.

WAT Lipolysis Is Essential for Thermogenesis During Fasting

When BAT-KO mice can use dietary nutrients to fuel thermogenesis in the fed state, they must rely on endogenous fuel during fasting. Fasting mobilizes energy stores mainly by inducing hepatic glycogenolysis and WAT lipolysis. It has been shown that mice lacking ATGL globally or in all adipose tissues are cold sensitive (Ahmadian et al., 2011; Haemmerle et al., 2006) suggesting a critical role of adipose lipolysis in cold-induced thermogenesis. During fasting, mice lacking CGI-58 in BAT only were not cold sensitive (Figure 2). Given this, we hypothesized that WAT lipolysis is essential for fueling thermogenesis during fasting. To test this hypothesis, we created a mouse line with CGI-58 inactivation in both BAT and WAT (FAT-KO mice) (Figure S5A). FAT-KO mice showed no alterations in weight gain and food intake despite increased fat body mass and weights of all adipose depots (Figure 5A-D). Like BAT-KO mice, FAT-KO mice also showed an enlarged white fat-looking iBAT (Figure 5E) and large cytosolic LD deposition in iBAT adipocytes (Figure 5F) resulting in increased brown adipocyte size (Figure 5G). Relative to controls, they also had increased total amounts of DNA and protein per iBAT (Figure S5B). As expected, FAT-KO mice were completely resistant to lipolysis stimulation (Figure 5H). Failure of an adrenergic agonist to stimulate lipolysis in FAT-KO mice demonstrates an essential role of CGI-58 in mediating the stimulated lipolysis. Like mice lacking ATGL globally (Haemmerle et al., 2006), FAT-KO mice housed at ambient temperature also developed hypothermia during fasting (Figure 5I). They were cold sensitive when food was removed during cold exposure (Figure 5J). Since mice lacking CGI-58 in BAT only were not cold sensitive during fasting, our results suggest that it is the WAT lipolysis that fuels thermogenesis in these animals in the fasted state.

Despite cold intolerance during fasting, FAT-KO mice were able to tolerate cold when they were provided food during cold exposure (Figure 5J) suggesting that inhibiting adipose lipolysis causes cold intolerance by limiting thermogenic fuels, not by impairing thermogenic machinery. In FAT-KO mice fed a HFD, a chow diet, or a chow diet coupled with β3 agonist treatment, iBAT levels of UCP1 protein and mRNA did not decrease when normalized to GAPDH (Figure 5K, 5L, and S5C), and the levels actually elevated when considering the relative total amounts of DNA and protein per iBAT depot (Figure S5B). In HFD-fed mice treated with CL316,243, we did see a lower level of UCP1 protein in the CGI-58-deficient iBAT after normalization to GAPDH (Figure S5D). Again, when considering the relative total amounts of protein per iBAT, the total amount of UCP1 protein was largely unchanged in the CGI-58-deficient iBAT depot. However, unlike BAT-KO mice, FAT-KO mice had a drastic reduction in thermogenic capacity as evidenced by blunted increases in core body temperatures (Figure S5E) and oxygen consumption after treatment with CL316,243 at thermoneutrality (Figure S5F and S5G). Thus, WAT lipolysis plays a key role in determining whole-body thermogenic capacity.

CGI-58 Deletion in BAT Stimulates WAT Browning

Cold-exposed BAT-KO mice relative to controls exhibited higher body temperatures when they were provided food during cold exposure (Figure 2). It appeared that BAT-KO mice had a higher set point of whole-body thermogenesis in the brain, which could activate multiple compensatory thermogenic mechanisms through SNS. We did observe increased protein expression of TH, a marker for sympathetic innervation, in iBAT (Figure 3D) and iWAT (Figure 6A). WAT browning is an important cold adaptative mechanism often induced by sympathetic activation. Indeed, BAT-KO versus control mice housed at room temperature (a moderate cold condition compared to thermoneutrality), exposed to cold, or treated with the β3 agonist CL316,243 for 4 days all showed augmented WAT browning as evidenced by increased emergence of adipocytes containing multilocular LDs and enhanced UCP1 immunohistochemical staining in iWAT (Figure 6B and 6C), a fat pad sensitive to browning factors. Increased WAT browning of BAT-KO mice was further supported by elevated UCP1 mRNA and protein levels in iWAT after chronic cold exposure or β3 agonist treatment (Figure 6D and 6E). Under the basal condition (22°C and saline treatment), UCP1 mRNA levels in iWAT also increased significantly in BAT-KO mice when Student-*t*-test, not Two-way ANOVA, was used for statistical analysis (Figure 6D).

UCP1 transcription in beige adipocytes may activate UCP1-cre recombinase, resulting in excision of floxed CGI-58 alleles. CGI-58 protein expression levels in iWAT decreased modestly in BAT-KO mice after cold or β3 agonist stimulation (Figure 6A and 6E), but this does not answer whether CGI-58-floxed alleles were excised in beige adipocytes because of un-browned white adipocytes present in this depot. To circumvent this issue, we crossed BAT-KO mice with Rosa26-eYFP reporter mice (Srinivas et al., 2001). In these mice, UCP1 promoter activation resulted in excision of the loxP-floxed STOP sequence before eYFP, allowing eYFP expression and tracking of UCP1-positive beige adipocytes. Immunostaining of CGI-58 in iWAT sections revealed that CGI-58 expression disappeared from only a small proportion of eYFP-positive beige adipocytes in BAT-KO mice (Figure S6A). This observation suggests that UCP1-cre is less efficient in beige than brown adipocytes in

excising floxed CGI-58 alleles, which is consistent with previous studies using the same UCP1-cre mouse line (Altshuler-Keylin et al., 2016; Kong et al., 2014). Given the normal UCP1 expression in CGI-58-deficient iBAT (Figure 3), our results indicate that UCP1 expression or beige adipocyte recruitment is not coupled with CGI-58 expression, which may imply that the stimulated adipose LD lipolysis is dispensable for UCP1 expression or WAT browning.

Mitochondrial respiration capacity is expected to be higher in thermogenic beige adipocytes than classical white adipocytes. To determine if this is the case in BAT-KO mice, we measured oxygen consumption of iWAT cell suspensions. As expected, the iWAT live cell suspension from BAT-KO mice relative to controls had significantly elevated basal and maximum oxygen consumption rates (Figure S6B), indicating that beige adipocytes in BAT-KO mice are functionally active.

Adipose browning can be induced by increased sympathetic innervation and/or direct actions of humoral and hormonal factors on adipocytes. TH protein levels in iWAT increased in BAT-KO mice housed at room temperature or exposed to the cold for 7 days (Figure 6A). The iWAT mRNA for β3 adrenergic receptor also elevated in these mice (Figure S6C). Thus, defective LD lipolysis in BAT may enhance WAT browning by increasing sympathetic innervation. To examine this possibility, we chemically and selectively denervated the sympathetic nerves by injecting the catecholaminergic neurotoxin 6-hydroxydopamine (6-OHDA) into one of two iWAT pads as described (Vaughan et al., 2014). Surgical denervation was not chosen because it cuts both sensory and sympathetic nerves. Ten days after 6-OHDA injection and cold exposure, TH protein levels in the denervated fat pad relative to the shamed operated pad of the same mouse decreased 56% and 60% in control and BAT-KO mice, respectively, which was associated with 62% and 69% decreases of UCP1 protein levels in the respective groups (Figure S6D). Consistently beige adipocytes in the denervated iWAT fat pad decreased substantially as revealed by H&E staining and UCP1 immunostaining (Figure S6E and S6F). These results suggest that WAT browning depends largely on sympathetic innervation, and that the increased sympathetic innervation into iWAT explains, in a large part, the increased WAT browning in BAT-KO mice.

CGI-58 Deletion in BAT Improves Metabolic Profile in Mice

Energy-dissipating adipocytes contribute significantly to handling of lipids and glucose in humans and mice (Bartelt et al., 2011; Cohen et al., 2014; Orava et al., 2011; Ouellet et al., 2012; Stanford et al., 2013). To examine whether selective inhibition of LD lipolysis in BAT has any impact on overnutrition-induced metabolic disorders, we fed BAT-KO and control mice a HFD. Relative to littermate controls, BAT-KO mice had improved glucose tolerance (Figure 7A), and increased insulin sensitivity as evidenced by increased Quantitative Insulin Sensitive Check Index (QUICKI) due to significantly reduced plasma insulin and a trend towards reduction of plasma glucose (Figure 7B and 7C). Reduced plasma insulin levels in BAT-KO mice were not a result of impaired insulin secretion as plasma insulin levels in both genotypes responded similarly to arginine and glucose challenges (Figure 7D and 7E). Besides glucose and insulin, serum concentrations of triglycerides, total cholesterol, and FFAs remained unchanged in BAT-KO mice (Figure 7F and 7G) except serum leptin that

decreased significantly (Figure 7H) likely due to reduced WAT mass (Figure 1H). Adipose tissue energy homeostasis critically regulates fat deposition in non-adipose tissues such as liver. Overnutrition often induces hepatic steatosis. We found that inhibiting LD lipolysis in BAT reduced liver weight and hepatic contents of lipids, including triglycerides and cholesterol in HFD-fed mice (Figure 7I and 7J). Our results collectively suggest a healthier metabolic profile in BAT-KO mice than controls.

Discussion

Cytosolic LD lipolysis in adipocytes is often stimulated by sympathetic activation. This stimulated lipolysis in brown adipocytes is situated at the crossroad of cold-induced nonshivering thermogenesis (Cannon and Nedergaard, 2004), but its *in vivo* significance has not been examined in whole animals. In this study, we demonstrate that LD lipolysis in brown adipocytes is not essential for cold-induced thermogenesis in mice regardless of food availability. Mice defective in the stimulated lipolysis in BAT had normal thermogenic capacity. Relative to littermate controls, they had higher body temperatures when they were provided food during cold exposure. Inhibiting LD lipolysis in BAT reprogramed BAT to combust more glucose and perhaps FFAs from the blood and stimulated WAT browning. Our findings demonstrated that LD lipolysis in BAT is not energetically critical for heat production, but plays an important role in regulating BAT fuel sources and WAT thermogenesis during cold adaptation. Our comparative studies of BAT-KO and FAT-KO mice revealed an essential role of WAT lipolysis in fueling thermogenesis during fasting.

Global and adipose ATGL knockout mice are cold sensitive (Ahmadian et al., 2011; Haemmerle et al., 2006). Simultaneously inhibiting intracellular lipolysis in both WAT and BAT using nicotinic acid (niacin) causes cold intolerance in humans and rodents (Blondin et al., 2017; Doi et al., 1979; Labbe et al., 2015). While these studies established a critical role of total adipose lipolysis in cold-induced thermogenesis, they did not distinguish the specific effect of BAT and WAT lipolysis on thermoregulation. In addition, all of these studies were performed with the experimental subjects having no access to food during cold exposure, and it remained unclear whether inhibiting total adipose lipolysis causes cold intolerance in the fed state. We found that FAT-KO mice lacking CGI-58 in both BAT and WAT are not cold sensitive when they were provided food during cold exposure. Similar results were obtained in mice lacking ATGL in both BAT and WAT (Schreiber, 2017). Given that mice lacking CGI-58 or ATGL (Schreiber, 2017) in BAT only are not cold sensitive under both fasted and fed conditions, our findings demonstrated that LD lipolysis-deficient BAT is capable of producing heat as long as thermogenic fuels are not limited.

Muscle shivering contributes significantly to whole-body thermogenesis when total fat lipolysis is inhibited by niacin or UCP1 ablation (Blondin et al., 2017; Golozoubova et al., 2001). We acclimated our mice for a week prior to cold exposure to minimize the effect of muscle shivering so that the role of lipolysis in different adipose tissues in thermoregulation can be assessed. Importantly, we examined whole-body thermogenic capacity in BAT-KO and FAT-KO mice by injecting the β3 agonist CL316,243 under a thermoneutral zone that eliminated muscle shivering. While the thermogenic capacity was largely maintained in BAT-KO mice, it was severely impaired in FAT-KO mice. This happened when the total

amount of UCP1 protein per iBAT depot was actually increased due to iBAT recruitment in these two animal models. Thus, the availability of thermogenic substrates from WAT lipolysis, such as FFAs, seems to have a bigger role than the total UCP1 protein per BAT depot in determining the magnitude of β3 agonist-induced oxygen consumption in mice, which is consistent with a previous study showing that β3 adrenergic receptor expressed in WAT plays a predominant role in determining total energy expenditure levels following CL316,243 injection (Grujic et al., 1997). Our data therefore support a key role of WAT lipolysis in thermoregulation in mice.

An interesting finding in this study was the increased browning of WAT in BAT-KO mice. Mice with BAT paucity (Schulz et al., 2013) or hamsters with iBAT sympathetic denervation (Nguyen et al., 2016) also had enhanced WAT browning, but this may be due to a general loss of BAT functions or thermogenic stimulation. Here we revealed a different mechanism in regulation of WAT browning, *i.e.*, selectively inhibiting LD lipolysis in BAT through CGI-58 deletion was sufficient to stimulate WAT browning without compromising BAT's thermogenic capacity. Our findings thus establish CGI-58-mediated LD lipolysis in BAT as an important regulator of WAT thermogenesis.

In general, beige adipocytes in the browned WAT are originated from *de novo* adipogenesis of precursor cells and/or transdifferentiation of existing mature white adipocytes. Although the origin of beige adipocytes in BAT-KO mice has yet to be defined, iWAT levels of TH protein and β3 adrenergic receptor mRNA elevated, implying a potential role of neural signals in mediating WAT browning in BAT-KO mice. Defective LD lipolysis induced by CGI-58 ablation in brown adipocytes may activate the central nervous system by altering cells' normal metabolism, signaling pathways, neural circuits, and/or humoral/hormonal regulations. BAT and WAT have the sympathetic-sensory feedback circuits that converge in the central nervous system to sense fat lipolysis and regulate the sympathetic outflow during thermogenesis (Garretson et al., 2016; Ryu et al., 2015). BAT-KO mice had increased body temperatures during cold exposure, supporting some changes of body temperature set point in the brain. Although we cannot exclude potential roles of non-neural factors, such as BAT-derived batokines (Kajimura et al., 2015; Wu et al., 2013), our chemical denervation studies suggested an important role of the sympathetic innervation in mediating iWAT browning in BAT-KO mice.

BAT-KO mice appeared to be metabolically healthier than littermate controls. One simple explanation was that more circulating nutrients, such as glucose, were channeled to the recruited BAT and the browned WAT for heat production in these animals, resulting in less nutrients flowing to other tissues including liver for deposition. While this explanation seemed to be contrary to a recent report that nicotinic acid-induced inhibition of whole-body intracellular lipolysis reduces BAT uptake of ^{11}C-acetate and ^{18}F-fluorodeoxyglucose tracers in cold-exposed humans (Blondin et al., 2017), the human study may not represent a direct effect of lipolysis inhibition in BAT on its lipid and glucose uptake because other vital organs such as heart may compete with BAT for tracer uptake when WAT lipolysis was also inhibited. CGI-58-deficient iBAT expressed increased levels of Glut1 mRNA and had increased glucose uptake per depot when WAT lipolysis was intact. Increased levels of Glut1 mRNA and protein were also observed in CGI-58-deficient muscle, macrophages and

cultured cancer cells (Miao et al., 2014; Ou et al., 2014; Xie et al., 2015), and thus may reflect a cell autonomous metabolic adaptation when energy stores in cytosolic LDs cannot be mobilized for utilization. This cell autonomous effect, together with the recruited BAT and the browned WAT, likely increased whole-body glucose disposal capacity in BAT-KO mice, which may explain why a bolus of glucose only induces a modest rise in blood glucose in these animals during cold exposure. Collectively, our studies suggest that selective inhibition of LD lipolysis in BAT may be a viable approach for improving metabolic health, which, unlike inhibition of lipolysis in all adipose tissues, will not compromise body's thermogenic capacity.

Contact for Reagent and Resource Sharing

Further information and requests for reagents may be directed to the Lead Contact, Liqing Yu (lyu68@gsu.edu).

Experimental model and Subject Details

Mice

Brown adipose-specific CGI-58 knockout (BAT-KO) mice were produced by crossing CGI-58-floxed mice generated in our lab previously (Guo et al., 2013) with B6.FVB-Tg (Ucp1-cre) 1 Evdr/J mice (The Jackson Laboratory, Stock #: 024670) generated by Dr. Evan Rosen's lab at Harvard Medical School. The Ucp1-cre mice specifically express cre recombinase in UCP1 positive cells, leading to selective inactivation of gene expression in brown and beige adipocytes (Kong et al., 2014). Homozygous CGI-58 floxed mice without Ucp1-cre transgene were used as controls for all experiments.

Whole adipose tissue CGI-58 knockout (FAT-KO) mice were generated by crossing our CGI-58-floxed mice with adiponectin-cre mice [B6;FVB-Tg(Adipoq-cre)1Evdr/J mice, The Jackson Laboratory, Stock #: 010803] generated by Dr. Evan Rosen (Eguchi et al., 2011). The adiponectin-cre mice express cre recombinase in all adipose tissues, thus inactivating gene expression in whole adipose tissue. Homozygous CGI-58 floxed mice without adiponectin-cre transgene were as controls for all experiments.

Mice were housed in a pathogen-free animal facility at 22°C with a 12 h light/dark cycle from 6AM to 6PM and fed *ad libitum* a standard chow diet (LabDiet) or a high fat diet (HFD) containing 60% energy from fat, 20% energy from carbohydrate, and 20% energy from protein (D12492, Research Diets Inc.). Diet treatments and weight measurements were started at 6 weeks of age. The specific age of the mice for each experiment is indicated in the figure legend. All animal experiments were performed with male mice and approved by the Institutional Animal Care and Use Committees (IACUC) at the University of Maryland at College Park and at Georgia State University.

Method Details

Metabolic Phenotyping and Telemetry

Indirect Calorimetry (Oxymax/ CLAMS, Columbus Instruments, Columbus, OH) was used to measure energy expenditure, respiratory exchange ratio (RER), and physical activity in mice at 22°C and 30°C. The core body temperature was continuously monitored by Telemetry (Mini Mitter/Philips Respironics, Bend, OR; ER4000 energizer/receivers, G2 E-mitters implanted intraperitoneally). Rectal temperature was monitored in some mice subjected to acute cold exposure using Thermalert TH-5 device (Physitemp). Food intake was measured in metabolic chambers. Body composition was determined by using by EchoMRI-100H Body Composition Analyzer (EchoMRI LLC). We allowed 2-4 days of acclimation to different housing environment and temperature conditions.

Lipase Activity Assays

Tissue lipase activity was assayed as described previously (Wei et al., 2007). Snap-frozen iBATs were quickly weighed, homogenized in ice-cold buffer (50 mM Tris-HCI, pH 7.4, 250 mM sucrose, 1 mM EDTA), and sonicated briefly. Protein contents in homogenates were analyzed using a BCA kit. Lipase activity was initiated by mixing 20 μl of homogenates containing 1 μg of total proteins, 10 μl of 5 μM 4-mtehylumbelliferyl heptanoate (4-MUH) for assays using HSL inhibitor 0079-1A (NovoNordisk), or 2 μg of total proteins and 20 μl of 10 μM 4-MUH for assays including ATGL inhibitor Atglistatin (Cat.#: 1469924-27-3, Cayman), in Reaction Buffer (20 mM Tris-HCI, pH 8.0, 1 mM EDTA, 300 μM taurodeoxycholate), and 60 μl of Reaction Buffer in 96-well-plates and incubating at room temperature with shaking for 5 min. The fluorescence was then continuously recorded over a 10 min-period at 355 nm as excitation and 460 nm as emission wavelengths at 22°C in a plate reader.

In vivo Lipolysis Assays

The mice were injected intraperitoneally with isoproterenol at 10 mg/kg body weight around 10AM. Plasma samples were collected before and 15 min after isoproterenol injection. Plasma concentrations of FFA and glycerol were analyzed using Free Fatty Acids, Half Micro Test kit (Cat.#: 11383175001, Roche), or NEFA-HR (2) (Cat.#: 434-91795 and 434-91995, Wako Diagnostics) and Free Glycerol Reagent (Sigma).

Chronic CL-316,243 Treatment

CL-316,243 at 1 mg/kg body weight or saline were injected into mice daily around 10AM for 4 days. On day 5, the mice were sacrificed around 1PM without additional injection.

Ex vivo Lipolysis Assays

The iBATs of BAT-KO and control mice were surgically removed and washed with PBS. Tissue pieces (~12 mg) were preincubated in DMEM containing 40 μM Atglistatin or vehicle DMSO for 8 h at 37°C, or 10 μM HSL inhibitor 0079-1A (NovoNordisk) or vehicle DMSO for 1 h at 37°C. Thereafter, the medium was replaced by DMEM containing 2% fatty acid-free BSA in the presence or absence of 20 μM forskolin and 40 μM Atglistatin or 10

µM HSL inhibitor, and incubated for an additional 60 min at 37°C. The medium was then collected for FFA assays using NEFA-HR (2) (Wako Diagnostics).

Immunohistochemistry

The iWAT was fixed in 10% formalin solution, paraffin-embedded, and then sectioned at 5 µm thickness. The sections were deparaffinized and rehydrated, followed by antigen retrieval using 10 mM sodium citrate (pH6.0) for 20min. After antigen retrieval, non-specific sites were blocked by incubating the sections in TBS containing 10% normal goat serum and 0.2% Tween 20 for 40 min. The sections were then incubated with a primary antibody against UCP1 (1:200) for overnight at 4°C, followed by three washes, 5 min each, with TBS-Tween 20 solution and incubation for 1h with a biotinylated secondary antibody (1:200) included in VECTASSTAIN Elite ABC HRP Kit (Peroxidase, Rabbit IgG (Cat.#: PK-6101, Vector Laboratories). After three washes, the sections were incubated with the reagents in VECTASSTAIN Elite ABC HRP Kit for 30 min and then with 3,3′-diaminobenzidine tetrahydrochloride (DAB) (Thermo Scientific Pierce) for 5-10 min. After three washes, cell nuclei were stained with hematoxylin (Ricca Chemical Company). The sections were dehydrated, sealed, and examined under a microscope.

Glucose Disposal and Insulin Sensitivity Tests

For glucose tolerance test (GTT), the mice were fasted overnight (16 h) and then injected *i.p.* with glucose solution at 1.5 g/kg body weight. Blood glucose concentrations were measured using Bayer Contour Glucometer (Bayer Healthcare, LLC.) at 0, 15, 30, 60, and 120 min after glucose injection. For glucose-stimulated insulin secretion, plasma samples were collected during GTT and plasma insulin concentrations were measured (Millipore). For insulin tolerance test (ITT), the mice were fasted for 6 h during the daytime cycle, followed by an intraperitoneal injection of recombinant human insulin in saline at a dose of 0.75 U/kg body weight. Blood glucose levels were monitored at 0, 15, 30, 60 and 120 min after insulin injection.

Analysis of Adipocyte Size

The adipose tissue cell sizing was done in osmium-fixed urea-isolated adipocytes as described previously (Etherton et al., 1977) with some modifications. Briefly, the adipose tissues from different fat depots of the mice on HFD for 17 weeks were excised aseptically, sliced to ~50 mg in size and rinsed twice in 0.154 M NaCl at 37°C to wash off free lipids on the tissues. The tissue slices were transferred to scintillation vials containing 1.2 mL of 50mM Colloidine HCl buffer and 2 mL of 3% osmium tetroxide in 0.05 M Colloidine HCl buffer (pH 7.4 at 37°C). The sample vials were kept in a ventilated fume hood at room temperature for 72 h. The osmium-colloidine buffer was removed and replaced by 10 mL of 0.154 M NaCl for 24 h. Subsequently, 10 mL 8M Urea in 0.154 M NaCl was added to the sample vials and the vials were intermittently swirled by hand and kept in room temperature for 48 h. This solubilized the connective tissue in the adipose tissue slices resulting in a suspension of adipocyte cells. The adipocyte cell suspension was passed through 250 µM nylon membrane to remove any of the remaining tissue debris. The cells were rinsed with 0.01% Triton-X in distilled water and then used to profile cell size distribution using Multisizer® Coulter Counter (Beckman coulter Ireland Inc.).

Tissue Lipid Analysis

Total lipids were extracted as described previously (Temel et al., 2007). To determine tissue lipid concentrations, a total of ~40-50 mg of tissue was sliced and extracted with 1:1 $CHCl_3$/ MeOH. The organic phase was analyzed for lipid species. Enzymatic assays were used to determine total cholesterol (TC), free cholesterol (FC), and triglyceride (TG) concentrations of the samples. TC and FC were measured with enzymatic assay kit from Wako (Cat.#: 439-17501 for TC and Cat.#: 435-35801 for FC, Wako). TG was measured enzymatically using the Free Glycerol Reagent (Cat.#: F6428, Sigma-Aldrich) and Triglyceride Reagent (Cat.#: T2449, Sigma-Aldrich). Protein concentrations in the delipidated samples were determined using a Lowry assay (Lowry et al., 1951).

Glucose Uptake Assays

To measure insulin-stimulated glucose uptake, the mice were fasted overnight (16h), and then injected with human insulin at 0.75 mU/Kg and 10 μCi of C^{14}-2-Deoxyglucose (2-DG). Forty-five minutes after 2-DG injection, the mice were sacrificed and tissues collected. For cold-induced glucose uptake, overnight fasted mice were exposed to cold (4°C) for 30 min before injection of 10 μCi of $[^3H]$-2-DG as a tracer and then sacrificed for tissue collection after additional 45 min cold exposure. DG is transported into tissues and phosphorylated to 2-deoxyglucose 6-phosphate (2-DGP). Tissue contents of 2-DGP were used to reflect their glucose uptake efficiency. To determine tissue 2-DGP content, samples were homogenized and 2-DGP was separated from 2-DG using ion exchange column (Chromatography Columns #731-6211, Bio Rad), and then counted as described (Kim et al., 2000).

Protein Extraction and Immunoblotting

The tissues were homogenized and lysed for 30 min in RIPA buffer containing 0.1% SDS with a protease and phosphatase inhibitor cocktail (Sigma), followed by sonication and centrifugation. To avoid fat contamination, a $26G_{1/2}$ syringe was used to collect the supernatant. The protein concentration of the supernatant was determined using a bicinchoninic acid (BCA) kit (BCA, Pierce, Rockford, IL). For immunoblotting, proteins in the supernatant were denatured by heating, separated by SDS-PAGE, and then transferred onto a nitrocellulose membrane (Bio-Rad). The membrane was incubated in a 5% non-fat milk blocking buffer (TBS-Tween 20) for 1 h, followed by incubation with a primary antibody in TBS-Tween 20 containing 5%BSA for overnight at 4°C. After 3 washes with TBS-Tween 20, the membrane was incubated with a secondary antibody, washed, and developed with Enhanced Chemiluminescence Detection Reagents (ECL, Thermo Fisher). The protein signals were imaged using a Bio-Rad ChemiDoc System.

Quantitative Real-time Polymerase Chain Reaction

Total RNAs were isolated using TRIzol® Reagents. RNAs were reverse transcribed into cDNA using TaqMan® Reverse Transcription Reagents (Applied Biosystems) and tissue mRNA levels were determined by qPCR using Stratagene Mx3005p PCR machine (Agilent Technologies). Reactions were done in duplicate for each biological sample using SYBR® Green Real-Time PCR Master Mix (Invitrogen). The relative mRNA expression level for

each gene was calculated by the $2^{(-DDCt)}$ method and normalized to GAPDH, which was arbitrarily set to 1.

Primer	Forward (5′ to 3′)	Reverse (5′ to 3′)
CD36	GGAACTGTGGGCTCATTGC	CATGAGAATGCCTCCAAACAC
Dio2	GTCCGCAAATGACCCCTTT	CCCACCCACTCTCTGACTTTC
FATP1	CCGTATCCTCACGCATGTGT	CTCCATCGTGTCCTCAATGAC
Glut1	GGTGTGCAGCAGCCTGTGTA	CAACAAACAGCGACACCACAGT
Glut4	CCGGCAGCCTCTGATCAT	CCGACTCGAAGATGCTGGTT
LPL	ACTCTGTGTCTAACTGCCACTTCAA	ATACATTCCCGTTACCGTCCAT
PGC-1α	GACTCAGTGTCACCACCGAAA	TGAACGAGAGCGCATCCTT
PRDM16	CAGCACGGTGAAGCCATTC	GCGTGCATTCGCTTGTG
PPAR-α	GCCTGTCTGTCGGGATGT	GGCTTCGTGGATTCTCTTG
PPAR-γ	GCCCTTTGGTGACTTTATGGA	GCAGCAGGTTGTCTTGGATG
UCP1	AAGCTGTGCGATGTCCATGT	AAGCCACAAACCCTTTGAAAA
β₃AR	TCCTTCTACCTTCCCCTCCTT	CGGCTTAGCCACAACGAACAC
GAPDH	ACCACAGTCCATGCCATCAC	CACCACCCTGTTGCTGTAGCC

Arginine Tolerance Test (ATT)

Mice were fasted for 6 h and then injected *i.p.* with arginine in saline at 1 g/kg body weight. Plasma insulin concentrations were measured using Ultra-Sensitive Mouse Insulin ELISA Kit (Crystal Chem) at 0, 5, 15, 30 min after arginine injection.

Chemical Denervation of the Sympathetic Nerves in iWAT Pads

Chemical denervation of sympathetic nerves in the iWAT was performed using the catecholaminergic neurotoxin 6-hydroxy-dopamine hydrochloride (6-OHDA) as described (Vaughan et al., 2014). Briefly, 6-OHDA was prepared at 9 mg/ml in 0.15 M NaCI containing 1% ascorbic acid. A total of 24 μl (2 μl per injection at 12 loci) of 6-OHDA solution was injected into the right side iWAT pad per mouse and a total of 24 μl of vehicle was injected into the left side iWAT pad as a shamed operated control. For the determination of the effect of sympathetic innervation on iWAT browning, prior to denervation, the mice were housed at thermoneutrality (30°C) for 3 weeks to minimize the basal level differences in WAT browning between BAT-KO and control mice. After denervation, the mice were recovered at thermoneutrality for 7 days and then at room temperature for 3 days, followed by 6 days of the intermittent cold exposure (12 h at 4°C in the light cycle and 12 h at room temperature during the dark cycle). Twenty-four hours before sacrifice, the mice were housed at 4°C continuously to maximally induce browning. All of the mice survived this cold exposure regimen after iWAT sympathetic denervation.

Seahorse Analysis of Primary Brown Adipocytes

Primary brown adipocytes were prepared from the stromal vasculature fraction (SVF) isolated from iBAT. In brief, iBAT was isolated and digested with PBS containing 10 mM $CaCl_2$, Collagenase D (1.5 U/ml) and Dispase II (2.4 U/ml) for ~45 min. After digestion, the SVF was collected by centrifugation at $700 \times g$ for 10 min at 37°C, and then filtered through a 40 μm nylon mesh cell strainer. The cells in the SVF were cultured in the Maintaining

Medium (DMEM/F12 supplemented with 10% FBS). For Seahorse studies, 20,000 cells were plated onto each well of XF96 Cell Culture Microplates. When the cells reached at ~95% confluency, the induction medium [1 nM 3,3′5-Triiodo-L-thyronine (T3), 5 μg/ml insulin, 125 μM indomethacin, 2 μg/ml dexamethasone, 0.5 mM 3-isobutyl-1-methyxanthine (IBMX), 0.5 μM rosiglitazone] was added. After 48 h induction, the cells were maintained in the Maintaining Medium supplemented with insulin (5 μg/ml), T3 (1 nM), and rosiglitazone (0.5 μM) for additional 48 h induction. The cells were fully differentiated and used for Seahorse analysis after additional 3-4 days of incubation in the fresh Maintaining Medium containing Insulin (5 μg/ml), T3 (1 nM), and rosiglitazone (1 μM).

XF^{e}96 Extracellular Flux Analyzer was used for Seahorse studies. Briefly, the basal respiration was recorded in the untreated cells, followed by inhibition of the coupled respiration by oligomycin (1 μM). The sympathetic activation-associated uncoupled respiration was then measured after addition of isoproterenol (1 μM). The maximum respiration capacity of the cells was assessed after addition of 2 μM carbonyl cyanide-4-(thfluomrthoxy)phenylhydrazone (FCCP). Lastly, non-mitochondrial respiration was measured after addition of rotenone/antimycin A (0.5 μM).

Oxygen Consumption Rates of Live Cell Suspensions of iWATs

The iWATs from 10-week-old BAT-KO and control mice were collected and digested in PBS containing 10 mM $CaCl_2$, Collagenase D (1.5 U/ml) and Dispase II (2.4 U/ml) at 37°C for 40 min. The cell suspensions were then used directly for Seahorse analysis. The basal and maximal oxygen consumption rates were normalized by the DNA amount in each cell suspension preparation.

Calculation of Quantitative Insulin Sensitive Check Index (QUICKI)

Plasma insulin and glucose concentrations were determined in overnight fasted BAT-KO and control mice. QUICKI was calculated as 1 / [log(fasting insulin at μU/ml) + log(fasting glucose at mg/dL)].

Quantification and Statistical Analysis

Data are expressed as Mean ± SEM, and were tested for statistical significance by Two-way ANOVA with Bonferroni *post hoc* tests when both genotypes and treatments were considered, One-way ANOVA with Tukey's *post hoc* tests when multiple groups were compared, or Student f-tests when the two groups were compared. The assumption of normality was tested using a Shapiro-Wilks test. The *p* value less than 0.05 was considered statistically significant. Data were analyzed using GraphPad Software 5.0 (Graphpad). The statistical parameters can be found in the figure legends. For all Figures, $*p < 0.05$ and $**p < 0.01$ vs. genotype on the same diet; $^\#p < 0.05$ vs. treatment of the same genotype.

Data Availability

The raw images are deposited and accessible at Mendeley (doi:10.17632/r7t3jt9sxk.4).

Supplementary Material

Refer to Web version on PubMed Central for supplementary material.

Acknowledgments

References

Ahmadian M, Abbott MJ, Tang T, Hudak CS, Kim Y, Bruss M, Hellerstein MK, Lee HY, Samuel VT, Shulman GI, et al. Desnutrin/ATGL is regulated by AMPK and is required for a brown adipose phenotype. Cell Metab. 2011; 13:739–748. [PubMed: 21641555]

Altshuler-Keylin S, Shinoda K, Hasegawa Y, Ikeda K, Hong H, Kang Q, Yang Y, Perera RM, Debnath J, Kajimura S. Beige Adipocyte Maintenance Is Regulated by Autophagy-Induced Mitochondrial Clearance. Cell Metab. 2016; 24:402–419. [PubMed: 27568548]

Bartelt A, Bruns OT, Reimer R, Hohenberg H, Ittrich H, Peldschus K, Kaul MG, Tromsdorf UI, Weller H, Waurisch C, et al. Brown adipose tissue activity controls triglyceride clearance. Nat Med. 2011; 17:200–205. [PubMed: 21258337]

Blondin DP, Frisch F, Phoenix S, Guerin B, Turcotte EE, Haman F, Richard D, Carpentier AC. Inhibition of Intracellular Triglyceride Lipolysis Suppresses Cold-Induced Brown Adipose Tissue Metabolism and Increases Shivering in Humans. Cell Metab. 2017; 25:438–447. [PubMed: 28089568]

Cannon B, Nedergaard J. Brown adipose tissue: function and physiological significance. Physiol Rev. 2004; 84:277–359. [PubMed: 14715917]

Cohen P, Levy JD, Zhang Y, Frontini A, Kolodin DP, Svensson KJ, Lo JC, Zeng X, Ye L, Khandekar MJ, et al. Ablation of PRDM16 and beige adipose causes metabolic dysfunction and a subcutaneous to visceral fat switch. Cell. 2014; 156:304–316. [PubMed: 24439384]

Cypess AM, Lehman S, Williams G, Tal I, Rodman D, Goldfine AB, Kuo FC, Palmer EL, Tseng YH, Doria A, et al. Identification and importance of brown adipose tissue in adult humans. N Engl J Med. 2009; 360:1509–1517. [PubMed: 19357406]

Doi K, Ohno T, Kurahashi M, Kuroshima A. Thermoregulatory nonshivering thermogenesis in men, with special reference to lipid metabolism. Jpn J Physiol. 1979; 29:359–372. [PubMed: 533941]

Fischer J, Lefevre C, Morava E, Mussini JM, Laforet P, Negre-Salvayre A, Lathrop M, Salvayre R. The gene encoding adipose triglyceride lipase (PNPLA2) is mutated in neutral lipid storage disease with myopathy. Nat Genet. 2007; 39:28–30. [PubMed: 17187067]

Foster MT, Bartness TJ. Sympathetic but not sensory denervation stimulates white adipocyte proliferation. Am J Physiol Regul Integr Comp Physiol. 2006; 291:R1630–1637. [PubMed: 16887921]

Garretson JT, Szymanski LA, Schwartz GJ, Xue B, Ryu V, Bartness TJ. Lipolysis sensation by white fat afferent nerves triggers brown fat thermogenesis. Mol Metab. 2016; 5:626–634. [PubMed: 27656400]

Golozoubova V, Hohtola E, Matthias A, Jacobsson A, Cannon B, Nedergaard J. Only UCP1 can mediate adaptive nonshivering thermogenesis in the cold. FASEB J. 2001; 15:2048–2050. [PubMed: 11511509]

Grujic D, Susulic VS, Harper ME, Himms-Hagen J, Cunningham BA, Corkey BE, Lowell BB. Beta3-adrenergic receptors on white and brown adipocytes mediate beta3-selective agonist-induced effects on energy expenditure, insulin secretion, and food intake. A study using transgenic and gene knockout mice. J Biol Chem. 1997; 272:17686–17693. [PubMed: 9211919]

Guo F, Ma Y, Kadegowda AK, Xie P, Liu G, Liu X, Miao H, Ou J, Su X, Zheng Z, et al. Deficiency of liver Comparative Gene Identification-58 causes steatohepatitis and fibrosis in mice. J Lipid Res. 2013; 54:2109–2120. [PubMed: 23733885]

Haemmerle G, Lass A, Zimmermann R, Gorkiewicz G, Meyer C, Rozman J, Heldmaier G, Maier R, Theussl C, Eder S, et al. Defective lipolysis and altered energy metabolism in mice lacking adipose triglyceride lipase. Science. 2006; 312:734–737. [PubMed: 16675698]

Haemmerle G, Moustafa T, Woelkart G, Buttner S, Schmidt A, van de Weijer T, Hesselink M, Jaeger D, Kienesberger PC, Zierler K, et al. ATGL-mediated fat catabolism regulates cardiac mitochondrial function via PPAR-alpha and PGC-1. Nat Med. 2011; 17:1076–1085. [PubMed: 21857651]

Honnor RC, Dhillon GS, Londos C. cAMP-dependent protein kinase and lipolysis in rat adipocytes. II. Definition of steady-state relationship with lipolytic and antilipolytic modulators. J Biol Chem. 1985; 260:15130–15138. [PubMed: 3877723]

Jespersen NZ, Larsen TJ, Peijs L, Daugaard S, Homoe P, Loft A, de Jong J, Mathur N, Cannon B, Nedergaard J, et al. A classical brown adipose tissue mRNA signature partly overlaps with brite in the supraclavicular region of adult humans. Cell Metab. 2013; 17:798–805. [PubMed: 23663743]

Kajimura S, Spiegelman BM, Seale P. Brown and Beige Fat: Physiological Roles beyond Heat Generation. Cell Metab. 2015; 22:546–559. [PubMed: 26445512]

Kazak L, Chouchani ET, Jedrychowski MP, Erickson BK, Shinoda K, Cohen P, Vetrivelan R, Lu GZ, Laznik-Bogoslavski D, Hasenfuss SC, et al. A creatine-driven substrate cycle enhances energy expenditure and thermogenesis in beige fat. Cell. 2015; 163:643–655. [PubMed: 26496606]

Kong X, Banks A, Liu T, Kazak L, Rao RR, Cohen P, Wang X, Yu S, Lo JC, Tseng YH, et al. IRF4 is a key thermogenic transcriptional partner of PGC-1alpha. Cell. 2014; 158:69–83. [PubMed: 24995979]

Kozak UC, Kopecky J, Teisinger J, Enerback S, Boyer B, Kozak LP. An upstream enhancer regulating brown-fat-specific expression of the mitochondrial uncoupling protein gene. Mol Cell Biol. 1994; 14:59–67. [PubMed: 8264627]

Labbe SM, Caron A, Bakan I, Laplante M, Carpentier AC, Lecomte R, Richard D. In vivo measurement of energy substrate contribution to cold-induced brown adipose tissue thermogenesis. FASEB J. 2015; 29:2046–2058. [PubMed: 25681456]

Lass A, Zimmermann R, Haemmerle G, Riederer M, Schoiswohl G, Schweiger M, Kienesberger P, Strauss JG, Gorkiewicz G, Zechner R. Adipose triglyceride lipase-mediated lipolysis of cellular fat stores is activated by CGI-58 and defective in Chanarin-Dorfman Syndrome. Cell Metab. 2006; 3:309–319. [PubMed: 16679289]

Li Y, Fromme T, Schweizer S, Schottl T, Klingenspor M. Taking control over intracellular fatty acid levels is essential for the analysis of thermogenic function in cultured primary brown and brite/beige adipocytes. EMBO Rep. 2014; 15:1069–1076. [PubMed: 25135951]

Liu P, Ying Y, Zhao Y, Mundy DI, Zhu M, Anderson RG. Chinese hamster ovary K2 cell lipid droplets appear to be metabolic organelles involved in membrane traffic. J Biol Chem. 2004; 279:3787–3792. [PubMed: 14597625]

Lord CC, Ferguson D, Thomas G, Brown AL, Schugar RC, Burrows A, Gromovsky AD, Betters J, Neumann C, Sacks J, et al. Regulation of Hepatic Triacylglycerol Metabolism by CGI-58 Does Not Require ATGL Co-activation. Cell Rep. 2016; 16:939–949. [PubMed: 27396333]

Ma SW, Foster DO. Uptake of glucose and release of fatty acids and glycerol by rat brown adipose tissue in vivo. Can J Physiol Pharmacol. 1986; 64:609–614. [PubMed: 3730946]

Miao H, Ou J, Ma Y, Guo F, Yang Z, Wiggins M, Liu C, Song W, Han X, Wang M, et al. Macrophage CGI-58 Deficiency Activates ROS-Inflammasome Pathway to Promote Insulin Resistance in Mice. Cell Rep. 2014; 7:223–235. [PubMed: 24703845]

Nedergaard J, Cannon B. The browning of white adipose tissue: some burning issues. Cell Metab. 2014; 20:396–407. [PubMed: 25127354]

Nguyen NL, Barr CL, Ryu V, Cao Q, Xue B, Bartness TJ. Separate and shared sympathetic outflow to white and brown fat coordinately regulate thermoregulation and beige adipocyte recruitment. Am J Physiol Regul Integr Comp Physiol. 2016; 312:14.

Orava J, Nuutila P, Lidell ME, Oikonen V, Noponen T, Viljanen T, Scheinin M, Taittonen M, Niemi T, Enerback S, et al. Different metabolic responses of human brown adipose tissue to activation by cold and insulin. Cell Metab. 2011; 14:272–279. [PubMed: 21803297]

Ou J, Miao H, Ma Y, Guo F, Deng J, Wei X, Zhou J, Xie G, Shi H, Xue B, et al. Loss of abhd5 promotes colorectal tumor development and progression by inducing aerobic glycolysis and epithelial-mesenchymal transition. Cell Rep. 2014; 9:1798–1811. [PubMed: 25482557]

Ouellet V, Labbe SM, Blondin DP, Phoenix S, Guerin B, Haman F, Turcotte EE, Richard D, Carpentier AC. Brown adipose tissue oxidative metabolism contributes to energy expenditure during acute cold exposure in humans. J Clin Invest. 2012; 122:545–552. [PubMed: 22269323]

Ozaki K, Sano T, Tsuji N, Matsuura T, Narama I. Carnitine is necessary to maintain the phenotype and function of brown adipose tissue. Lab Invest. 2011; 91:704–710. [PubMed: 21321536]

Petrovic N, Walden TB, Shabalina IG, Timmons JA, Cannon B, Nedergaard J. Chronic peroxisome proliferator-activated receptor gamma (PPARgamma) activation of epididymally derived white adipocyte cultures reveals a population of thermogenically competent, UCP1-containing adipocytes molecularly distinct from classic brown adipocytes. J Biol Chem. 2010; 285:7153–7164. [PubMed: 20028987]

Rosen ED, Spiegelman BM. What we talk about when we talk about fat. Cell. 2014; 156:20–44. [PubMed: 24439368]

Rosenwald M, Perdikari A, Rulicke T, Wolfrum C. Bi-directional interconversion of brite and white adipocytes. Nat Cell Biol. 2013; 15:659–667. [PubMed: 23624403]

Ryu V, Garretson JT, Liu Y, Vaughan CH, Bartness TJ. Brown adipose tissue has sympathetic-sensory feedback circuits. J Neurosci. 2015; 35:2181–2190. [PubMed: 25653373]

Schreiber RD, D C, Wongsiriroj N, Schoiswohl G, Huetter S, Feiler U, Sedej S, Schmidt A, Kolb D, Wolkhard G, Rosenwald M, Wolfrum C, Wolfrum C, Kershaw EE, Hoeks J, Schrauwen P, Haemmerle G, Zechner R. Lipolysis in BAT is not essential for thermogenesis in vivo. Cell Metab. 2017

Schulz TJ, Huang P, Huang TL, Xue R, McDougall LE, Townsend KL, Cypess AM, Mishina Y, Gussoni E, Tseng YH. Brown-fat paucity due to impaired BMP signalling induces compensatory browning of white fat. Nature. 2013; 495:379–383. [PubMed: 23485971]

Schweiger M, Schreiber R, Haemmerle G, Lass A, Fledelius C, Jacobsen P, Tornqvist H, Zechner R, Zimmermann R. Adipose triglyceride lipase and hormone-sensitive lipase are the major enzymes in adipose tissue triacylglycerol catabolism. J Biol Chem. 2006; 281:40236–40241. [PubMed: 17074755]

Shabalina IG, Petrovic N, de Jong JM, Kalinovich AV, Cannon B, Nedergaard J. UCP1 in brite/beige adipose tissue mitochondria is functionally thermogenic. Cell Rep. 2013; 5:1196–1203. [PubMed: 24290753]

Sidossis L, Kajimura S. Brown and beige fat in humans: thermogenic adipocytes that control energy and glucose homeostasis. J Clin Invest. 2015; 125:478–486. [PubMed: 25642708]

Srinivas S, Watanabe T, Lin CS, William CM, Tanabe Y, Jessell TM, Costantini F. Cre reporter strains produced by targeted insertion of EYFP and ECFP into the ROSA26 locus. BMC Dev Biol. 2001; 1:4. [PubMed: 11299042]

Stanford KI, Middelbeek RJ, Townsend KL, An D, Nygaard EB, Hitchcox KM, Markan KR, Nakano K, Hirshman MF, Tseng YH, et al. Brown adipose tissue regulates glucose homeostasis and insulin sensitivity. J Clin Invest. 2013; 123:215–223. [PubMed: 23221344]

Subramanian V, Rothenberg A, Gomez C, Cohen AW, Garcia A, Bhattacharyya S, Shapiro L, Dolios G, Wang R, Lisanti MP, et al. Perilipin A mediates the reversible binding of CGI-58 to lipid droplets in 3T3-L1 adipocytes. J Biol Chem. 2004; 279:42062–42071. [PubMed: 15292255]

Sztalryd C, Komaromy MC, Kraemer FB. Overexpression of hormone-sensitive lipase prevents triglyceride accumulation in adipocytes. J Clin Invest. 1995; 95:2652–2661. [PubMed: 7769105]

Thonberg H, Fredriksson JM, Nedergaard J, Cannon B. A novel pathway for adrenergic stimulation of cAMP-response-element-binding protein (CREB) phosphorylation: mediation via alpha1-adrenoceptors and protein kinase C activation. Biochem J. 2002; 364:73–79. [PubMed: 11988078]

van Marken Lichtenbelt WD, Vanhommerig JW, Smulders NM, Drossaerts JM, Kemerink GJ, Bouvy ND, Schrauwen P, Teule GJ. Cold-activated brown adipose tissue in healthy men. N Engl J Med. 2009; 360:1500–1508. [PubMed: 19357405]

Vaughan CH, Zarebidaki E, Ehlen JC, Bartness TJ. Analysis and measurement of the sympathetic and sensory innervation of white and brown adipose tissue. Methods Enzymol. 2014; 537:199–225. [PubMed: 24480348]

Virtanen KA, Lidell ME, Orava J, Heglind M, Westergren R, Niemi T, Taittonen M, Laine J, Savisto NJ, Enerback S, et al. Functional brown adipose tissue in healthy adults. N Engl J Med. 2009; 360:1518–1525. [PubMed: 19357407]

Wu J, Bostrom P, Sparks LM, Ye L, Choi JH, Giang AH, Khandekar M, Virtanen KA, Nuutila P, Schaart G, et al. Beige adipocytes are a distinct type of thermogenic fat cell in mouse and human. Cell. 2012; 150:366–376. [PubMed: 22796012]

Wu J, Cohen P, Spiegelman BM. Adaptive thermogenesis in adipocytes: is beige the new brown? Genes Dev. 2013; 27:234–250. [PubMed: 23388824]

Wu Q, Kazantzis M, Doege H, Ortegon AM, Tsang B, Falcon A, Stahl A. Fatty acid transport protein 1 is required for nonshivering thermogenesis in brown adipose tissue. Diabetes. 2006; 55:3229–3237. [PubMed: 17130465]

Xie P, Kadegowda AK, Ma Y, Guo F, Han X, Wang M, Groban L, Xue B, Shi H, Li H, et al. Muscle-Specific Deletion of Comparative Gene Identification-58 (CGI-58) Causes Muscle Steatosis but Improves Insulin Sensitivity in Male Mice. Endocrinology. 2015; 156:1648–1658. [PubMed: 25751639]

Yamaguchi T, Omatsu N, Matsushita S, Osumi T. CGI-58 interacts with perilipin and is localized to lipid droplets. Possible involvement of CGI-58 mislocalization in Chanarin-Dorfman syndrome. J Biol Chem. 2004; 279:30490–30497. [PubMed: 15136565]

Zhao J, Unelius L, Bengtsson T, Cannon B, Nedergaard J. Coexisting beta-adrenoceptor subtypes: significance for thermogenic process in brown fat cells. Am J Physiol. 1994; 267:C969–979. [PubMed: 7943293]

Highlights

- The stimulated lipolysis in BAT is not essential for cold-induced thermogenesis

- Mice defective in adipose lipolysis are not cold sensitive when food is present

- Inhibiting stimulated BAT lipolysis by CGI-58 deletion induces WAT browning

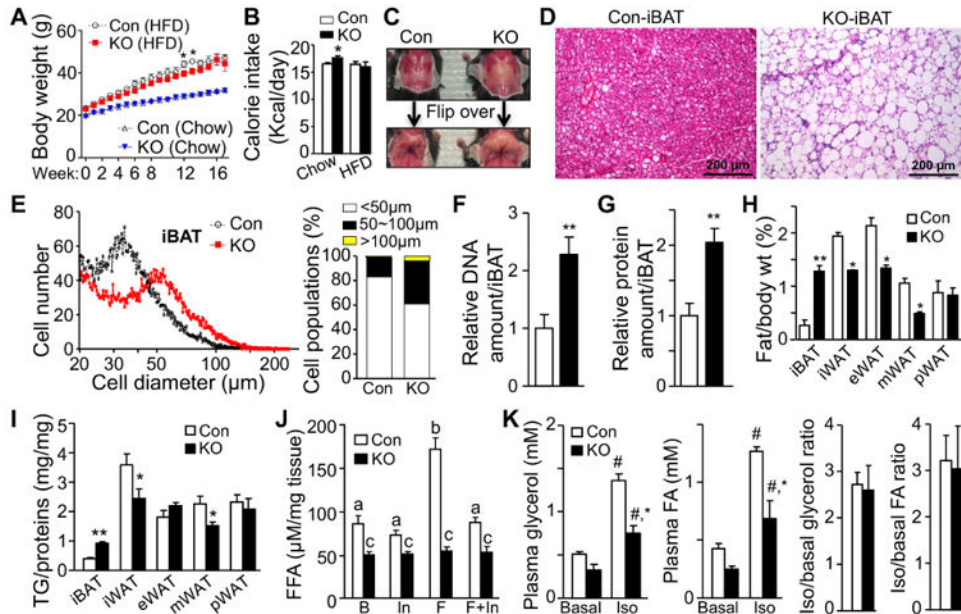- WAT lipolysis is essential to defend body temperature during fasting

Figure 1. Selective Inactivation of CGI-58 in BAT Induces Steatotic Hypertrophy and Hyperplasia and Blocks the Stimulated Lipolysis in iBAT

The data in this figure were obtained from the mice housed at room temperature (22°C).

(A) Weight gain of 6-week-old (Week 0) BAT-KO (KO) and control (Con) mice subjected to chow (n = 10/group) or HFD (n = 11/group).

(B) Food intake of mice on the fifth week of chow (n = 6/group) or HFD (n = 11/group).

(C) Gross appearance of iBATs in 24-week-old mice on chow diet.

(D) H&E staining of iBATs from 14-week-old chow-fed mice.

(E) Average brown adipocyte sizes in iBATs of mice on HFD for 18 weeks. For each mouse, 5,000 cells were measured. n = 5/group.

(F, G) Relative DNA and protein amounts per iBAT in 14-week-old mice on chow. n = 5/group.

(H) Adipose depot/body weight ratios (%) of mice on HFD for 5 weeks. n =7/group.

(I) The TG content in individual adipose depots of mice on HFD for 18 weeks. n = 5-7/group.

(J) Lipolysis assays of iBAT explants from 28-day-old mice. n = 5/group. B, basal; In, ATGL inhibitor Atglistatin; F, forskolin. Statistically significant differences are indicated by different small letters ($p < 0.05$, One-way ANOVA).

(K) *In vivo* lipolysis capacity of mice on HFD for 4 weeks. n = 5/group.
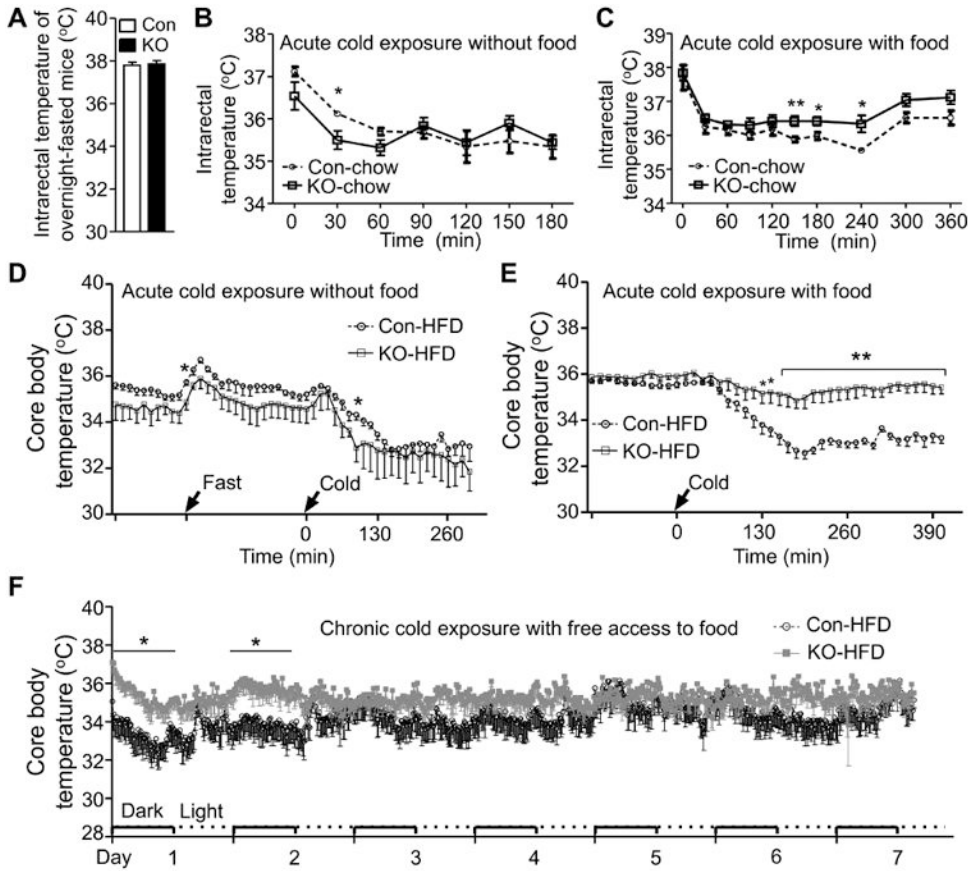
Figure 2. BAT-KO Mice Are Not Cold Sensitive

(A) Intrarectal temperatures of 20-week-old HFD-fed BAT-KO (KO) and control (Con) mice at 22°C. n = 4-5/group.

(B, C) Intrarectal temperatures of 10-11-week-old chow-fed mice exposed 4°C in the absence or presence of diet. n = 5/group.

(D) Core body temperatures of 28-week-old HFD-fed mice exposed to 4°C in the absence of food. n = 5-6/group.

(E) Core body temperatures of 24-week-old HFD-fed mice exposed to 4°C in the presence of food. n = 5-6/group.

(F) Core body temperatures of 18-week-old HFD-fed mice during 7 days of cold exposure. n = 6/group.
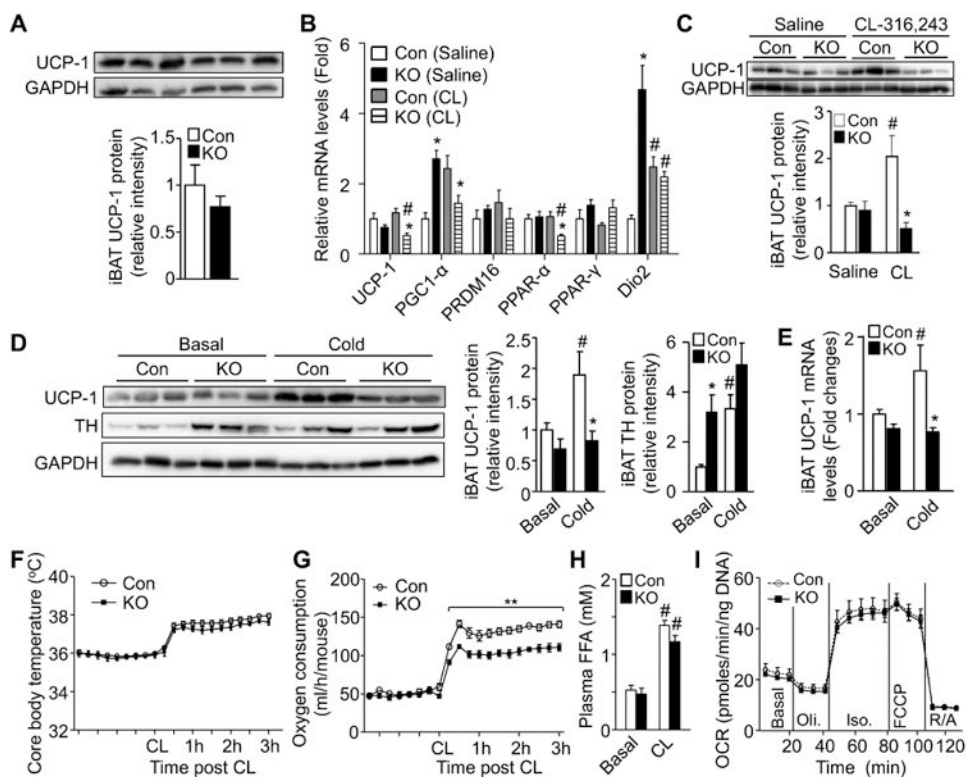
Figure 3. CGI-58 Deletion in BAT Does Not Reduce Whole-body Thermogenic Capacity

(A) Western blots and densitometry of iBAT UCP1 protein in 14-week-old chow-fed mice.

(B) Relative iBAT expression levels of thermogenesis-related genes from the mice injected with CL316,243 for 4 days (CL) or vehicle (Saline). n = 5/group.

(C) Western blots and densitometry of iBAT UCP1 in the same mice described under 3B.

(D) Western blots and densitometry analyses of iBAT UCP1 and TH proteins in 18-week-old HFD-fed mice at 22°C (Basal) or 4°C for 7 days (Cold).

(E) UCP1 mRNA levels in the iBAT of the mice described under 3D. n = 4-5/group.

(F and G) Core body temperatures (F) and oxygen consumption rates (G) in 23-week-old mice injected with a bolus of CL316,243 at thermoneutrality. n = 6/group.

(H) Plasma levels of FFAs in thermoneutrally housed 11-week-old mice at 15 min after a bolus of CL316,243 injection. n = 6-7/group.

(I) Oxygen consumption rates (OCRs) measured by Seahorse assays in isolated primary brown adipocytes from 28-day-old mice. Oli., oligomycin; Iso., isoproterenol; R/A, rotenone/antimycin.
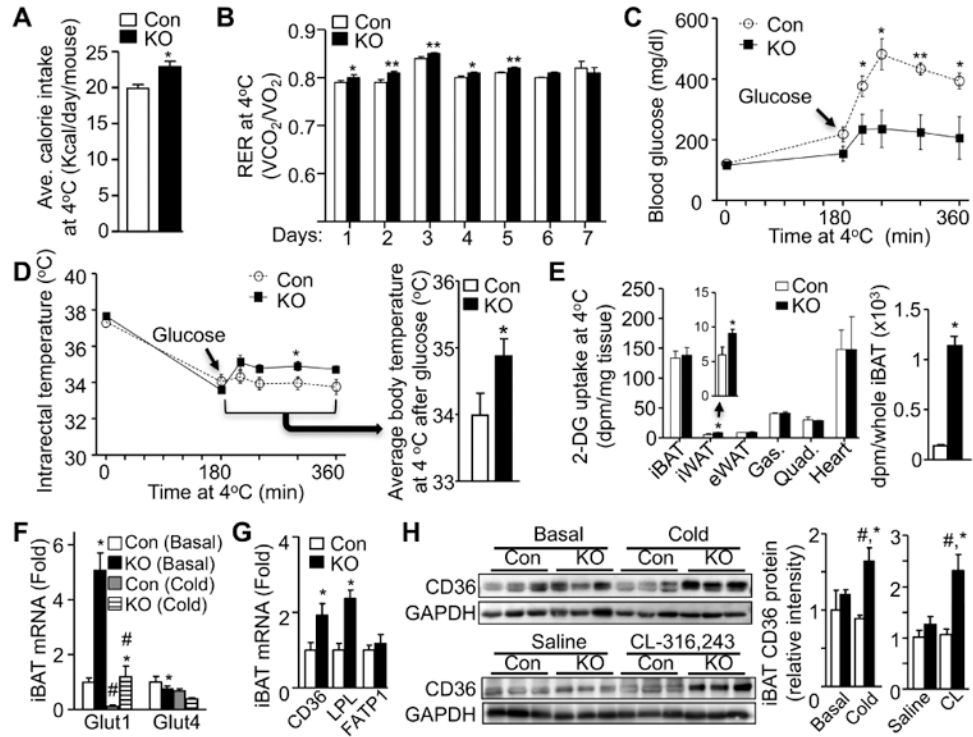
Figure 4. BAT-KO Mice Increase Combustion of Circulating Fuels During Cold Exposure

(A and B) Average daily calorie intake (A) and respiratory exchange ratio (RER) (B) of 18-week-old HFD-fed BAT-KO (KO) and control (Con) mice during 7 days of cold exposure. n = 5-6/group.

(C and D) Changes in blood glucose levels (C) and intrarectal temperatures (D) in 12-week-old HFD-fed mice after a bolus of glucose injection (*i.p.*, at 1.5 g/kg body weight). The mice were fasted for 7h (4h at room temperature and 3h at cold) prior to glucose injection. n = 4-5/group.

(E) Tissue glucose uptake in 20-week-old HFD-fed mice during acute cold exposure. The total glucose uptake of iBAT was calculated based on the total iBAT weight. n = 4-5/group.

(F) Levels of mRNAs for glucose transporter 1 (Glut1) and glucose transporter 4 (Glut4) in iBAT in mice housed at 22°C (Basal) or 4°C for 7 days (Cold). n = 5/group.

(G) Levels of mRNAs for CD36, lipoprotein lipase (LPL), and fatty acid transporter protein 1 (FATP1) in iBAT in 14-week-old HFD-fed mice housed at 22°C. n = 5/group.

(H) Immunoblots and densitometry of CD36 protein in iBAT in mice exposed to cold for 7 days or injected daily with CL316,243 for 4 days.
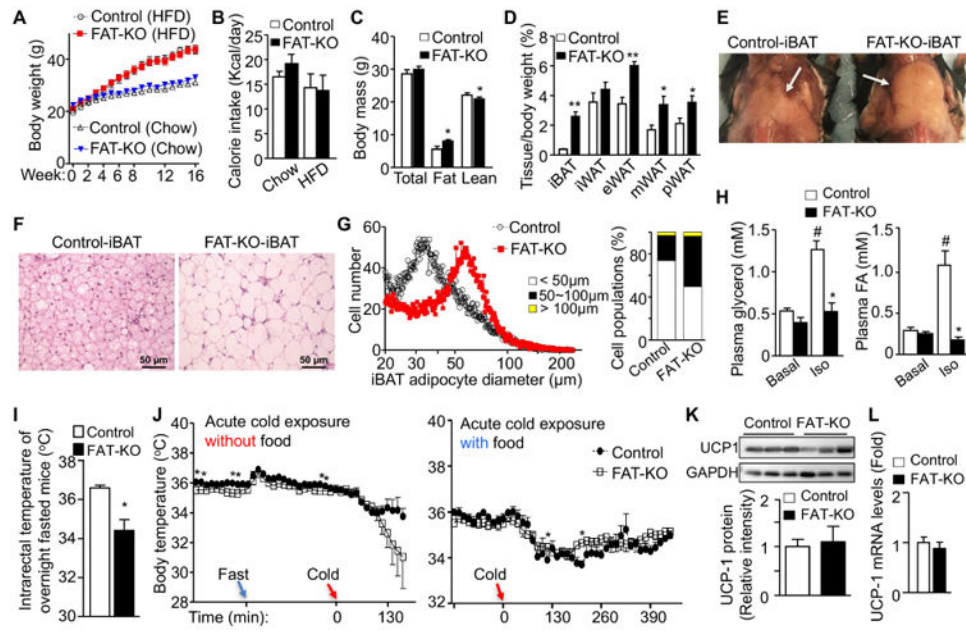
Figure 5. WAT Lipolysis Is Essential for Thermogenesis During Fasting

(A) Weight gain of FAT-KO and control mice on chow (n = 9-12) or HFD (n = 10-13. Mice were 6 weeks old at Week 0.

(B) Calorie intake on the fifth week of chow (n = 5-6/group) or HFD (n = 5-6/group) treatment.

(C) Body composition of 12-week-old HFD-fed mice. n = 6/group.

(D) Adipose depot/body weight ratios in 24-week-old HFD-fed mice. n = 7/group.

(E) Gross appearance of iBATs from 24-week-old HFD-fed mice.

(F) H&E staining of iBATs from 14-week-old HFD-fed mice.

(G) Adipocyte size of iBATs from 24-week-old HFD-fed mice. For each sample, 5,000 cells were measured. n = 5/group.

(H) *In vivo* lipolysis capacity of 10-week-old HFD-fed mice.

(I) Intrarectal temperatures of 26-week-old HFD-fed mice during cold exposure in the absence of food. n = 5-6/group.

(J) Core body temperatures of 23-week-old HFD-fed mice during cold exposure in the absence or presence of food. n = 5-6/group.

(K) Western blots and densitometry of UCP1 protein in iBAT in 22-week-old HFD-fed mice.

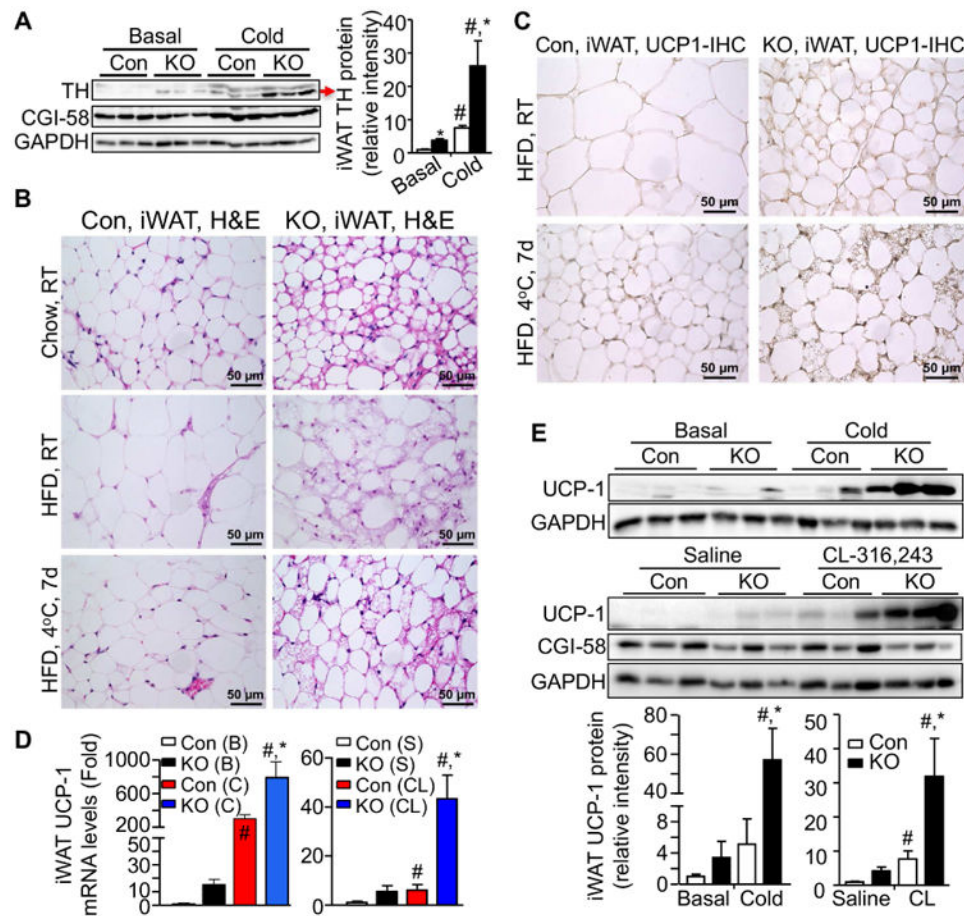(L) Levels of UCP1 mRNA in iBAT in 22-week-old HFD-fed mice. n = 4/group.

Figure 6. CGI-58 Deletion in BAT Stimulates WAT Browning

(A) Western blots and densitometry of tyrosine hydroxylase (TH) in iWAT in 18-week-old HFD-fed mice exposed to cold for 7 days.

(B) H&E staining of iWATs from 14-week-old chow-fed BAT-KO (KO) and control (Con) mice (top), 18-week-old HFD-fed mice (middle), and 18-week-old HFD-fed mice exposed to cold for 7 days (bottom).

(C) Immunostaining of UCP1 protein in iWAT in 18-week-old HFD-fed mice or 18-week-old HFD-fed mice exposed to cold for 7 days.

(D and E) Levels of UCP1 mRNA (D) and protein (E) in iWAT in 18-week-old HFD-fed mice at 22°C (Basal, or B) or 4°C for 7 days (Cold, or C) (n = 4-5/group), or 14-week-old HFD-fed mice injected with CL316,243 for 4 days (CL) or saline (S) (n = 5/group).
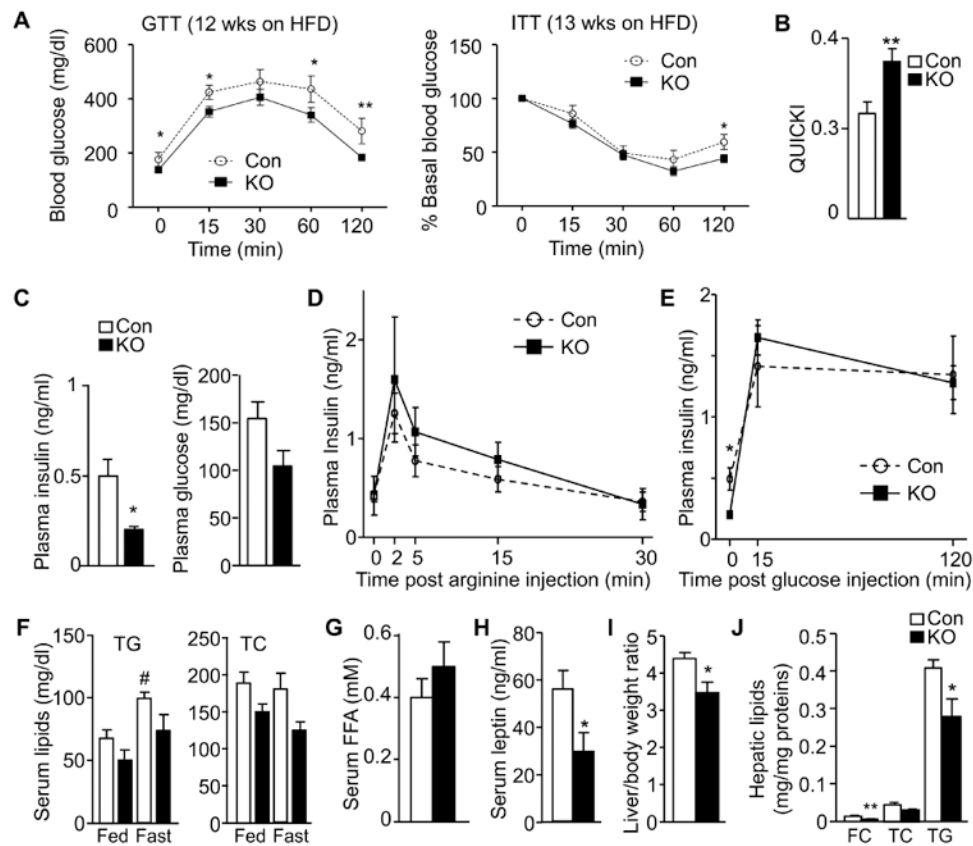
Figure 7. CGI-58 Deletion in BAT Improves Metabolic Profile in Mice

(A) Glucose tolerance test (GTT) and insulin tolerance test (ITT) in BAT-KO (KO) and control (Con) mice on HFD. n = 9-11/group.

(B) QUICKI insulin sensitivity indexes of overnight-fasted 17-week-old HFD-fed mice. N = 6/group.

(C) Plasma concentrations of insulin and glucose in 17-week-old HFD-fed mice fasted overnight. n = 6/group.

(D) Arginine-stimulated insulin secretion in 8-week-old mice. n = 6/group.

(E) Glucose-stimulated insulin secretion in 17-week-old HFD-fed mice. n = 6/group.

(F) Serum concentrations of triglycerides (TG) and total cholesterol (TC) in the fed or overnight-fasted 15-17-week-old HFD-fed mice. n = 6/group.

(G) Serum concentrations of FFAs in 17-week-old HFD-fed mice fasted overnight. n = 6/group.

(H) Serum concentrations of leptin in 15-week-old HFD-fed mice in the fed state. n = 6/group.

(I) Liver/body weight ratios in 24-week-old HFD-fed mice. n = 7/group.

(J) Hepatic contents of free cholesterol (FC), total cholesterol (TC), and TG in 24-week-old HFD-fed mice. n = 5/group.

Key Resources Table

REAGENT or RESOURCE	SOURCE	IDENTIFIER
Antibodies		
Rabbit polyclonal against UCP1	Abcam	AB10983
Rabbit polyclonal against GAPDH	Sigma-Aldrich	G9545
Mouse monoclonal against CGI-58	Abnova	H00051099-M01
Rabbit polyclonal against CD36	Abnova	PAB12463
Rabbit polyclonal against ATGL	Cayman Chemical	10006409
Rabbit polyclonal against HSL	Cell Signaling	4107T
Rabbit polyclonal against TH	Novous	NB300-109
Chemicals, Peptides, and Recombinant Proteins		
CL 316,243 disodium salt	Tocris	1499
Atglistatin (ATGL inhibitor)	Cayman Chemical	1469924-27-3
HSL inhibitor	NovoNordisk	0079-1A
Sodium Palmitate	Sigma-Aldrich	P9767
Formalin Solution, 10% (Histological)	Fisher Scientific	SF100
Triton X-100	Fisher Scientific	BP151
TWEEN 20	Fisher Scientific	BP337
SDS	Fisher Scientific	BP166
Sodium chloride	Fisher Scientific	S271
Tris-Base	Fisher Scientific	BP152
TRIZOL Reagent	Invitrogen	15-596-018
Sodium Pyruvate	Sigma-Aldrich	P5280
Rotenone	Sigma-Aldrich	557368
Antimycin A	Fisher Scientific	J63522
Carbonyl cyanide-4-(trifluoromethoxy)phenylhydrazone (FCCP)	Tocris	04-531-0
Isoproterenol hydrochloride	Sigma-Aldrich	I6504
Oligomycin	Tocris	4110
4-Methylumbelliferyl heptanoate	Sigma-Aldrich	M2514

REAGENT or RESOURCE	SOURCE	IDENTIFIER
Bovine serum albumin	Fisher Scientific	BP9706
Bovine serum albumin (fatty acid-free)	Sigma-Aldrich	A7030
3,3′-diaminobenzidine tetrahydrochloride (DAB substrate)	Thermo Fisher Scientific	PI34002
6-Hydroxy-dopamine hydrochloride	Sigma-Aldrich	H4381
L-Ascorbic acid	Fisher Scientific	A61
L-Arginine hydrochloride	Fisher Scientific	BP372
H^3-2-Deoxyglucose	PerkinElmer	NET328A001MC
C^{14}-2-Deoxyglucose	PerkinElmer	NEC720A050UC
Critical Commercial Assays		
Seahorse XF96 FluxPak mini	Seahorse Bioscience	102601-100
Ultra Sensitive Mouse Insulin ELISA Kit	Crystal Chem	90080
Sensitive Rat Insulin RIA	Millipore	SRI-13K
Triglyceride Reagent	Sigma-Aldrich	T2449
Free Glycerol Reagent	Sigma-Aldrich	F6428
NEFA-HR (2)	WAKO Diagnostics	434-91795 434-91995
Half Micro Test kit	Roche	1138317500
High-Capacity cDNA Reverse Transcription Kit	Applied Biosystems	4368814
Power SYBR Green PCR Mater Mix	Applied Biosystems	4367659
Quanti-iT™ dsDNA Assay Kit	Invitrogen	Q33120
VECTASSTAIN Elite ABC HRP Kit	Vector Laboratories	PK-6101
Experimental Models: Organisms/Strains		
Mouse: C57BL/6J	The Jackson Lab	000664
Mouse: B6FVB-Tg(UCP1-Cre)1Evdr/J	The Jackson Lab	024670
Mouse: B6.FVB-Tg(Adipoq-Cre)1Evdr/J	The Jackson Lab	010803
Mouse: B6.129X1-Gt(ROSA)26Sor^tm(EYFP)Cos/J	The Jackson Lab	006148
Software and Algorithms		
GraphPad Prism 5	GraphPad Software	http://graphpad.com
ImageJ Software	ImageJ	http://imagej.net
Wave 2.2.0	Agilent	http://www.agilent.com/en-us/support/cell-analysis-(seahorse)/seahorse-xf-software)

REAGENT or RESOURCE	SOURCE	IDENTIFIER
Image Lab™ Software	Bio-rad	http://www.bio-rad.com
Multisizer 3 Control Software	Beckman Coulter	774477
Raw Imaging Data	This paper	doi:10.17632/r7t3jt9sxk.4